The manuscript is published: Marilyne Philibert, Shuting Chen, Voon-Kean Wong, Kui Yao, Constantinos Soutis, and Matthieu Gresil, "Direct-write piezoelectric transducers on carbon-fiber reinforced polymer structures for exciting and receiving guided ultrasonic waves," IEEE Transactions on Ultrasonics, Ferroelectrics, and Frequency Control, DOI: 10.1109/TUFFC.2021.3073131, Vol. 68, No. 8, pp. 2733-2740, 2021.

Direct-write piezoelectric transducers on carbon-fiber reinforced polymer structures for exciting and receiving guided ultrasonic waves

Marilyne Philibert, Shuting Chen, Voon-Kean Wong, Kui Yao, Constantinos Soutis and Matthieu Gresil

***Abstract* — Advancements in the structural health monitoring (SHM) technology of composite materials are of paramount importance for early detection of critical damage. In this work, direct-write ultrasonic transducers (DWTs) were designed for the excitation and reception of selective ultrasonic guided waves and fabricated by spraying 25 µm thick piezoelectric poly(vinylidene fluoride-co-trifluoroethylene) (P(VDF-TRFE)) coating with a comb-shaped electrode on carbon fiber reinforced polymer (CFRP) plates. The characteristics and performance of the ultrasonic DWTs were benchmarked with the state-of-the-art devices, discrete lead zirconate titanate (PZT) ceramic transducers surface-mounted on the same CFRP plates. The DWTs exhibited improved Lamb wave mode excitation (A_0 or S_0 mode) relative to the discrete PZT transducers. Moreover, high signal-to-noise ratio was obtained by effectively cancelling other modes and enhancing the directivity with the periodic comb-shaped electrode design of the DWTs, despite the smaller signal amplitudes. The enhanced directivity overcompensates for lower amplitude attenuation, making DWT a good candidate for locally monitoring critical stress hot-spot regions in the CFRP structure prone to early damage initiation. Further, it is shown that pairing a DWT sensor with a discrete PZT actuator could further achieve balanced performance in both wave mode selection and signal amplitudes, making this combination really attractive for ultrasonic SHM.**

***Index Terms* — Composite material, direct write, ultrasonic transducer, Lamb wave, piezoelectric polymer, Structural Health Monitoring.**

I. Introduction

SINCE the 1980s with first applications of composites for primary aircraft structures, the sector has increased the content of composite materials leading to new lighter aircraft with more than half of its structural weight made of composites (A350, B787), projecting to satisfy the reduction of carbon dioxide emissions by half by 2050 relative to 2005 levels [1], [2]. This has motivated the community to develop novel cost-effective reliable methods for monitoring the structural integrity of composite materials. Of upmost importance is the effectiveness to detect and monitor barely visible impact damage (BVID) in carbon fiber reinforced polymer (CFRP), which significantly reduces mechanical properties and runs the risk of growing during service [3], [4]. Hence, its early detection merits investigation, as it would improve safety and reduce cost of repair. These objectives can be reached by structural health monitoring (SHM) techniques, using a permanently integrated distributed network of transducers able to continuously and autonomously monitor a structure, proved to be an efficient approach [2], [5]. A network of piezoelectric lead zirconate titanate (PZT) transducers can generate and sense guided waves travelling into large complex CFRP structures [6]–[8]. In particular, Lamb waves are divided into anti-symmetric A_n and symmetric S_n modes dominated by out-of-plane and in-plane displacement, respectively. Multiple modes unavoidably overlap in the signals acquired by ultrasonic transducers. Therefore, methods of mode selection have been implemented in ultrasonic SHM that can simplify signals, improving identification of a mode of interest and associated damage analysis. For instance, as only fundamental A_0 and S_0 modes exist at low frequency, they are often preferably selected by using the frequency corresponding to their highest amplitude response, which is typically linked to transducers length [2], [9]–[11]. Furthermore, the ability to select either A_0 or S_0 mode is profitable for damage detection and characterization qualification because they undergo different displacements, and hence respond distinctively to different damage. The S_0 mode is suitable for detection of damage in the thickness, whereas the A_0 mode is more sensitive to planar damage [2], [7], [9].

Moreover, it remains crucial to improve transducers integration and reliability maintaining low cost. Discrete ultrasonic transducers made of piezoelectric ceramic, such as

M. Philibert, S. Chen, V. K. Wong and K. Yao are with the Institute of Materials Research and Engineering, A*STAR (Agency for Science, Technology and Research), Singapore (email: k-yao@imre.a-star.edu.sg).

M. Philibert and C. Soutis are with the Department of Materials, The University of Manchester, UK. C. Soutis is also with the Aerospace Research Institute, The University of Manchester, UK.

M. Gresil is with the i-Composites Lab, Department of Materials Science and Engineering & Department of Mechanical and Aerospace Engineering, Monash University, Australia.

The work of Marilyne Philibert, Shuting Chen, Voon-KeanWong, and Kui Yao was supported in part by A*STAR, in part by RIE 2020 Advanced Manufacturing and Engineering (AME) SERC Strategic Funds under Grant A1718g0056, in part by RIE 2020 AME Industry Alignment Fund-Pre-Positioning (IAF-PP) under Grant A20F5a0043, and in part by the National Research Foundation Competitive Research Programme of Singapore under Grant NRF-CRP15-2015-04.

PZT, have been extensively studied because of their high piezoelectric strain coefficients. SHM networks of numerous distributed transducers and wiring can pose serious problems in aircrafts while adding a consequent weight to the structure. Less intrusive sensors such as embedded micro-fabricated sensors can overcome the issue [12], [13]. Meanwhile, present concerns about environment would tend to eliminate the use of lead or any heavy metals. Polymeric transducers are good candidates, adding the benefit of low process temperature and possible green solvent solution [14]. Their high flexibility allows them to be patterned on curved shape or limited space. In particular, poly(vinylidene fluoride) (PVDF) piezoelectric films have been developed for sensing applications [15]–[17]; its copolymer poly(vinylidene fluoride-co-trifluoroethylene) (P(VDF-TrFE)) is even more popular for coatings for its spontaneous crystallization into the ferroelectric β-phase [18]–[20]. Moreover, the PVDF density is less than ¼ the density of PZT.

Since SHM networks using discrete PZT transducers often imply costly and laborious manual installation, there is a desire of developing transducers using direct-write methods such as spraying or printing. Besides the high production efficiency, batch fabrication of direct-write transducers (DWT) promises for high consistency and enhanced mechanical strain coupling, by eliminating the need of bonding agent and reducing misalignments with structures [21]–[23]. Along with the improved system reliability, DWTs can be patterned on complex structures with minimized weight and profile. Recently, DWTs have been fabricated on metallic structures in our lab by spraying P(VDF-TrFE) [23]–[26]. However, ultrasonic-based SHM of CFRP are much more challenging than in metals because of anisotropy and numerous discontinuities due to their layered construction and higher wave attenuation, limiting its use at relatively lower frequencies [27], [28]. In literature, direct-write techniques have been used to deposit piezoelectric coating on CFRP structure using barium titanate (BT) [21] or PZT particles [22] in a polymer matrix; these sensors successfully detected acoustic emission from impact. This technique of passive sensing continuously monitors the structure capturing signals from unknown events, which is liable to various noise effects and makes signal interpretation hard.

In this work, we firstly focus on DWT design and fabrication of active P(VDF-TrFE) piezoelectric transducers on CFRP plates. Secondly, we explore DWTs performances and advantageous features in Lamb wave sensing and generation for SHM applications, in comparison with discrete PZT transducers. By investigating on A_0 mode attenuation, the DWT directivity feature makes them attractive for 'hot-spot' applications, monitoring critical location in the structure. Finally, the combination of PZT as actuator and DWT as sensor is explored with balanced improvement in both mode selection and signal-to-noise ratio.

II. Design and Fabrication of Direct-Write Transducers on CFRP

A. Direct-write transducer fabrication

As described in a previous work [29], the DWTs were made of a bottom electrode, a piezoelectric coating, and a top electrode, as illustrated in Fig. 1. Each of these layers were shaped using shadow masks. Unlike in previous work on metallic structures which can be directly used as ground electrode [23], an innovative silver nanowire bottom electrode was applied on the CFRP surface, which was previously sanded to improve adhesion. It is also uncertain how the chemical solvents will cause processing compatibility issues and piezoelectric property degradation for producing P(VDF-TrFE) coating on CFRP. A thin layer of silver nanowire dispersed in ethanol was sprayed and heated to 100 °C to form this ground electrode. The resistivity was measured to be less than 0.3 Ω/mm with good uniformity. Then, the P(VDF-TrFE) (72/28 mol%) coating was deposited on top of the bottom electrode, by spraying its dimethylformamide (DMF) and acetone solution, while heating at 90 °C, and followed by annealing at 135 °C. The thickness of the coating was measured to be about 25 μm with good homogeneity. The P(VDF-TrFE) coating was then poled by a non-contact corona discharge gun at 17 kV, forming an electrostatic surface charge of about 1000 V or higher. Finally, the top electrode made of silver conductive paste was patterned into comb-shape on top of the piezoelectric coating.

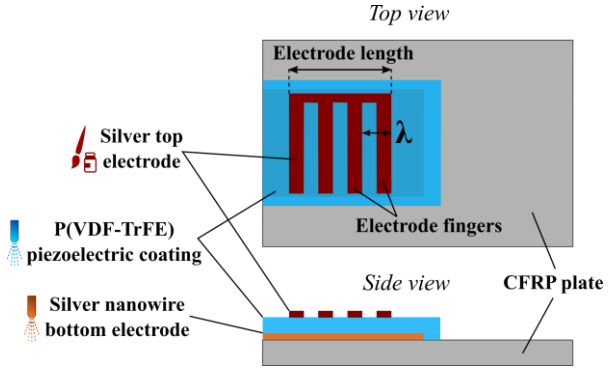

Fig. 1. Schematic illustration of a DWT fabricated on a CFRP plate: planar view (top) and side view (bottom schematic). The DWT has a comb-shaped electrode painted with four fingers of periodicity λ.

B. Lamb wave mode selection

The choice of a proper combination of frequency and mode on the dispersion curves is essential [30]. Dispersion curves show the presence of modes according to the thickness-frequency product. The mechanical properties of the quasi-isotropic CFRP plate of dimensions 250 mm × 225 mm × 2 mm, made of five woven plies were calculated from supplier information (details in Supplementary Information, Part I) and used for the calculation of the theoretical dispersion curves. With the assumptions of isotropic laminates and no damping, theoretical group velocities and phase velocities at low frequencies are plotted in Fig. 2. The comb-shaped pattern of the DWT top electrode was designed to select the desired Lamb wave modes at specific frequencies. This method for mode selection is very convenient, suitable and straightforward for

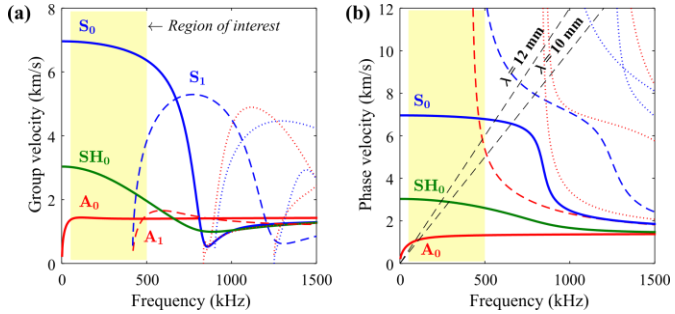

Fig. 2. Theoretical dispersion curves for our 2 mm thick CFRP plate studied showing velocities of Lamb wave antisymmetric modes in red and symmetric modes in blue, and shear horizontal mode in green: (a) group velocities and (b) phase velocities with two black dashed lines indicating two wavelengths. These lines are used to determine frequencies to select a mode for a fixed electrode periodicity in DWT.

TABLE I
THEORETICAL FREQUENCIES CORRESPONDING TO SPECIFIC WAVELENGTHS FOR A_0 AND S_0 MODES.

Wavelength (mm)	DWT minimum length* (mm)	Theoretical frequency for A_0 mode (kHz)	Theoretical frequency for S_0 mode (kHz)
8	20	148	762
10	25	112	656
12	30	88	560
20	50	42	344

* For a DWT with 3-finger electrode.

the novel direct-write fabrication of transducers from piezoelectric coatings. The fingers of the electrode match with the wavelength of the mode selected, by having a period of one wavelength (λ) and a width of half-wavelength ($\lambda/2$), as shown in Fig. 1 [31]–[33]. Increasing the number of fingers in the pattern, the purer the mode selection [34], [35]. A minimum of 3 fingers are required to create a "comb" shape electrode. Hence, electrode dimensions may be relatively large when using large wavelengths. A DWT minimum length is given in Table I, corresponding to a DWT with an electrode with 3 fingers ($3 \times (\lambda/2)$ for the 3 fingers + $2 \times (\lambda/2)$ for the space between fingers). Besides, fundamental Lamb wave modes are preferentially generated at low frequencies, below 500 kHz in our CFRP plate. This region of frequencies is used for its lower attenuation (lower frequencies), the almost constant group velocities that limit dispersion effects, and the reduced number of modes present simultaneously. A region of interest is highlighted in yellow in Fig. 2 corresponding to frequencies from 50 to 500 kHz. Table I provides theoretical frequencies that should be used to generate either A_0 mode or S_0 mode in the CFRP plate structure when using a specific wavelength. These values were obtained from dispersion curves of Fig. 2 (b). The wavelength, λ, of a mode was calculated with the phase velocity c_p through the equation:

$$\lambda = \frac{c_p}{f} \quad (1)$$

where f is the frequency. For comb transducers with a fixed electrode periodicity corresponding to the wavelength of the mode generated, the frequency to generate this mode was calculated with the same equation. Activation lines can be traced as in Fig. 2 (b) where two black dashed lines were traced as example, corresponding to wavelength of 10 mm and 12 mm. Intersections of these lines with the dispersion curves indicate the frequency to use to select a specific mode.

To explore different features of DWTs in comparison with discrete PZT transducers, multiple DWT samples were fabricated on distinct CFRP plates. The discrete PZT transducers, P-876.SP1 DuraAct (PI Ceramic Piezo Technology), with dimensions of 16 mm × 13 mm × 0.5 mm (insulation included) were glued on the sanded surface of the plate. Three CFRP plates were used in this study: Plate 1 with four PZT transducers, Plate 2 with pairs of DWTs of different top electrode periodicity, and Plate 3 with two pairs of PZTs and two pairs of DWTs of different electrode periodicity. Plate 1 and Plate 2 were used to compare the mode selection for PZT and DWT on same angle of wave propagation in the plate. On Plate 2, three periodicities of electrode were investigated: 8 mm, 10 mm and 12 mm. Plate 3 was used to compare PZT and DWT on a same plate with same distances between transducers and same angle of wave propagation in the plate. Plate 3 will be further investigated in Section III and IV.

C. Mode selection ability

Experiments were first conducted to study the ability of DWT to select A_0 mode using comb-shaped electrode patterns of different periodicities, in contrast with PZT transducers. Lamb wave signals were acquired such as signals were transmitted by a transducer (PZT or DWT) and received by another one located at a different position on the CFRP plate. The input signal was a five tone-burst sinusoidal signal with a Hanning window amplified to 100 Vpp (peak-to-peak voltage) and triggered every 10 milliseconds by a function generator Tektronix AFG3101. The received signals were collected with an oscilloscope Tektronix MDO3102 with an averaging of 512 acquisitions and then processed with Matlab. The signal processing included a band-pass filter with cut-off frequencies of ± 10 kHz of the frequency transmitted. Mode selection can be visually shown by plotting the tuning curve of the mode as in Fig. 3, which represents amplitudes of the mode obtained for different central frequency of excitation signal. Lamb waves were generated with central frequencies of excitation from 40

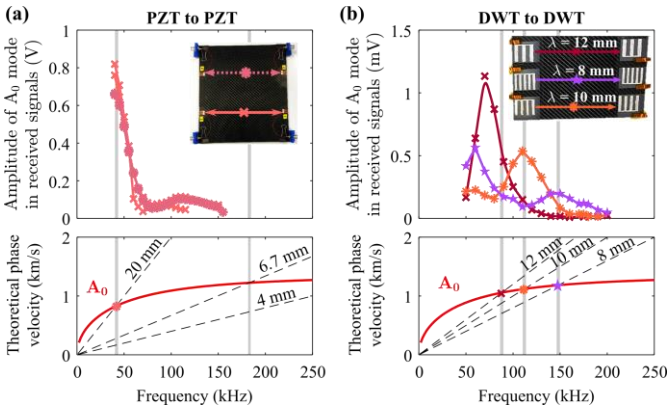

Fig. 3. Tuning curves representing A_0 mode amplitudes according to frequency of transmitted input signal for (a) discrete PZT transducers on Plate 1 and for (b) DWTs of different electrode patterns (periodicity of 12 mm, 10 mm, and 8 mm) on Plate 2. The bottom figures show theoretical phase velocity of A_0 mode with dashed lines indicating wavelengths, as in Fig. 2.

kHz to 200 kHz with increment of 10 kHz. From the time-of-flight of each wave packet appearing in envelopes of received signals, the group velocity was calculated and used to identify fundamental modes.

The A_0 mode was characterized with an experimental group velocity of about 1.2 km/s in experiments using Plate 1 with PZTs. The amplitudes of the A_0 mode generated and received by PZT were higher for frequencies below 100 kHz, as represented in tuning curves of Fig. 3 (a). It is known that a wavelength tuning occurs when the transducer's length is an odd multiple of the half-wavelength ($\lambda/2$) [2]. From technical data, the piezoelectric layer of the PZT was 10 mm × 10 mm. Thus, the possible wavelengths selected were 20 mm, 6.7 mm, 4 mm, etc. The activation lines of these 3 first values are plotted in dispersion curves of Fig. 3 (a) on the lower part; and corresponding theoretical frequencies to actuate A_0 are emphasized by grey lines. From Table I, the A_0 mode is generated at 42 kHz for a wavelength of 20 mm. In our experiments, the mode selection could not be proven by the PZT length because no data were taken at frequency lower than 40 kHz. No data were taken because there was no real interest for wavelengths larger than 20 mm and because the A_0 mode is highly dispersive with lower frequencies (region of interest highlighted in dispersion curves of Fig. 2). Therefore, the PZT length could partly explain the selection of A_0 mode at frequencies of 40 kHz or lower.

From experiments using DWTs on Plate 2, with an electrode periodicity of 12 mm, 10 mm and 8 mm, the A_0 mode was selected at 70 kHz, 110 kHz and 145 kHz respectively, as shown in Fig. 3 (b), close to theoretical values reported in Table I. The activation lines of these 3 wavelength values are plotted in dispersion curves of Fig. 3 (b) on the lower part; and corresponding theoretical frequencies to actuate A_0 are highlighted by grey lines. For the smallest wavelength, the higher amplitude of A_0 mode at low frequency (below 100 kHz) indicates the preferential excitation of the mode appearing with lower attenuation. With smaller wavelengths, the A_0 mode is associated to higher frequencies, and hence larger attenuation, which introduces a limitation in the use of mode selection. This can be corrected by improving performances of the DWT, for instance, by using larger electrode which enhances the excitation energy (larger capacitance). In this work, electrodes periodicity of 10 mm and 12 mm showed better results for mode selection than the 8 mm one, because they could activate the A_0 mode with higher amplitudes at their corresponding frequencies without being impacted by wave attenuation. In summary, the ability of DWT to effectively select the A_0 mode at different frequencies by means of control of periodicity in comb-shaped electrodes has been demonstrated. This ability is an attractive feature for SHM applications since it can simplify signals usually affected by modes superposition.

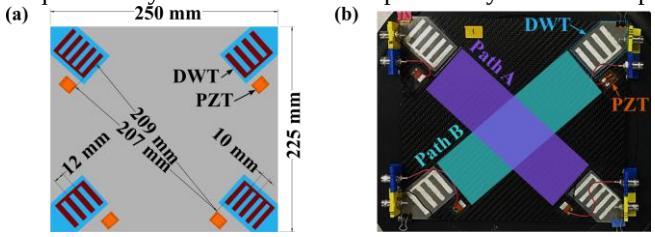

Fig. 4. (a) Design of the CFRP Plate 3 with position of four DWTs (in blue, with electrodes in red) and four discrete PZT transducers (in orange) on each corner of the plate (in grey); and (b) CFRP Plate 3 highlighting two paths: Path A and Path B, each path includes two PZTs and two DWTs. DWTs with electrode periodicity of 10 mm and 12 mm on Path A and Path B, respectively.

III. Direct-write transducer performances for SHM in comparison with PZT transducers

A. Plate design

Plate 3 is investigated to highlight the advantages of using DWTs, such as their ability to filter out unwanted modes, over PZTs. On this plate presented in Fig. 4, two pairs of DWTs were produced in two different patterns: 5 fingers electrode with periodicity of 10 mm on Path A and 4 fingers electrode with periodicity of 12 mm on Path B. The four DWTs were fabricated on each corner of the plate to cover the whole area and maximize the distance between actuator and sensor, and hence, allow modes to be more separated. Discrete PZTs were glued on the same CFRP plate right next to each of the DWT to let Lamb waves travel on the same respective paths.

B. Direct-write transducer response to guided wave

Signals were acquired with both pairs of DWTs on Plate 3 (Fig. 4). A baseline was taken over a wide range of central frequencies of signal excitation, from 40 to 550 kHz with increment of 5 kHz, and time domain signals were collected. By plotting each of these time domain signals according to their central frequency of excitation, plots were generated enlightening modes travelling at preferential frequencies, as represented in Fig. 5 (a) for either Path A or Path B. For example, plot for Path A in Fig. 5 (a) represents vertically aligned time domain signals collected from one of the DWT in

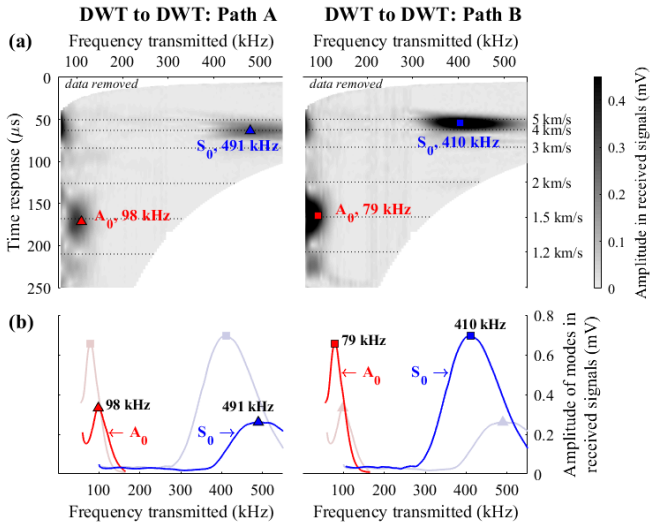

Fig. 5. (a) Envelopes of the received time domain signals plotted according to the central frequency of the transmitted input signal for guided waves travelling between DWTs with electrodes periodicity of 10 mm for Path A (left) and of 12 mm for Path B (right). White regions correspond to no data or removed data (electromagnetic interference). Dotted lines indicate the experimental group velocities. (b) Amplitudes of A_0 mode (in red) and S_0 mode (in blue) plotted according to the central frequency of the transmitted input signal for guided waves travelling between DWTs for Path A (left) and for Path B (right). Mode amplitudes for Path B and Path A are plotted again with dimmed lines on the left and on the right respectively.

Path A while the other DWT was transmitting an excitation signal. Each of these transmitted signals had a central frequency specified on the top of the plot. White regions in the plot correspond to no data or removed data attributed to electromagnetic interference. Fig. 5 (a) confirms that, for either Path A or Path B, both A_0 and S_0 modes appeared in signals received from and by DWTs. The experimental group velocities of A_0 was about 1.5 km/s. The experimental group velocities of S_0 were between 4 km/s and 4.6 km/s for 400 to 500 kHz. These experimental values are lower than theoretical values obtained between 6 km/s and 7 km/s in Fig. 2 (a), because of assumptions considered in calculation, such as isotropy. Besides, the distance between transducers (center to center) is influenced by non-negligible transducer size; group velocities calculated from time-of-flights using this distance might be altered.

From Fig. 5 (a) and the tuning curves of Fig. 5 (b), the ability of DWT to select fundamental Lamb wave modes by means of control of electrode periodicity was emphasized. For an electrode periodicity of 10 mm (Path A), the A_0 and S_0 modes were selected at 98 kHz and at 491 kHz, respectively. Likewise, for an electrode periodicity of 12 mm (Path B), the A_0 and S_0 modes were selected at 79 kHz and at 410 kHz respectively. Following the activation lines of Fig. 2 (b) obtained using (1), if A_0 is selected at 79 kHz for a wavelength of 12 mm, and at 98 kHz for a wavelength of 10 mm, its phase velocities are 0.95 km/s and 0.98 km/s respectively. Likewise, the phase velocities of S_0 are 4.92 km/s and 4 .91 km/s at 410 kHz and 491 kHz, respectively. The plots in Fig. 5 (a) show that single-mode guided wave excitation was achieved, seeing that only A_0 and S_0 appeared while other unwanted modes were filtered out. The downside of the use of DWT is that amplitudes of signals received were lower than 1 mV for a 100 Vpp signal generated upstream, due to small piezoelectric strain coefficient of P(VDF-TrFE). Nevertheless, the results of this study suggest that signals from DWT showed good signal-to-noise ratio for localized SHM. Single-mode excitation and reception was achieved, meaning only A_0 and S_0 modes appeared at their corresponding frequencies.

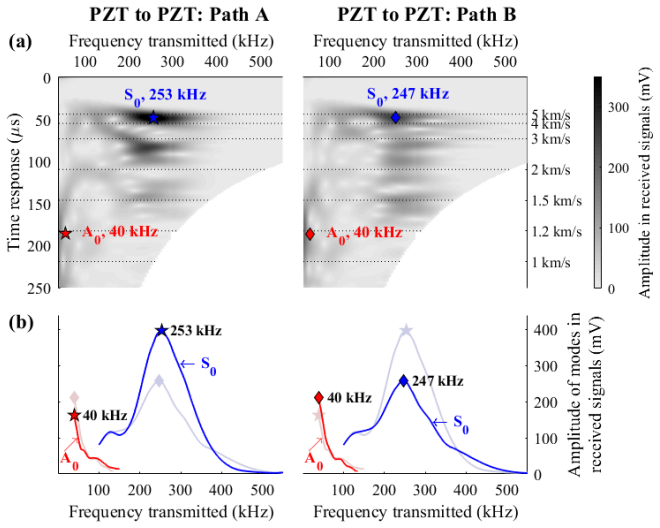

Fig. 6. (a) Envelopes of the received time domain signals plotted according to the central frequency of the transmitted input signal for guided waves travelling between discrete PZT transducers on Path A (left) and Path B (right). White regions correspond to no data or removed data. Dotted lines indicate the experimental group velocities. (b) Amplitudes of A_0 mode (in red) and S_0 mode (in blue) plotted according to the central frequency of the transmitted input signal for guided waves travelling between PZT for Path A (left) and Path B (right). Modes amplitudes for Path B and Path A are plotted again with dimmed lines on the left and on the right, respectively.

C. Comparison with discrete PZT transducer

Signals were acquired with both pairs of PZTs on Plate 3 (Fig. 4), as to compare with results observed for DWTs previously. The A_0 and S_0 modes were identified and appeared at frequencies below 70 kHz and between 200 and 300 kHz respectively, with group velocities of about 1.2 km/s and 4.6 km/s, respectively. Plots in Fig. 6 (a) show responses for PZT transducers. The A_0 mode appeared for low frequencies, hence large wavelengths, and is mixed with multiple other modes. It was observed that guided waves signals acquired from PZTs contained multiple modes existing simultaneously and overlapping, at any frequency. Whereas for DWTs, fundamental Lamb wave modes were clearly selected. The single-mode excitation and reception ability of DWT allowed to simplify signals and quickly visualize modes of interest.

The respective frequencies of the A_0 and S_0 modes generated and detected by PZTs are usually determined by the PZT length [2]. Globally, there was a main response between 200 and 300 kHz corresponding to the PZT resonance, as observed in Fig. 6 (a) in which the amplitudes of all wave packets were higher, and this deeply influenced the selection of the S_0 mode. Impedance changes at 259 and 286 kHz confirm resonance in the frequency region, as shown in Supplementary Information Fig. S-1, Part II. Nonetheless, from (1), assuming a wavelength of 20 mm related to the PZT length, the phase velocity of the S_0 mode at 250 kHz is 5 km/s. This value matches with the values of phase velocities calculated previously with DWTs (4.92 and 4.91 km/s at 410 and at 491 kHz, respectively), as the phase velocity of S_0 mode slightly decreases with frequency as represented in Fig. 2 (b). We know that theoretical dispersion curves in Fig. 2 and theoretical frequency values in Table I were higher than experimental ones because the theory did not consider wave attenuation. Confirming discussion in Section II-C, the PZT length might determine the frequencies of Lamb wave modes selection, and modes were selected with a wavelength of 20 mm, and enhanced amplitudes.

From Fig. 6 (a) and tuning curves of Fig. 6 (b), PZTs were proven not reliable, as they behaved substantially differently between Path A and Path B. Indeed, modes amplitudes were different from Path A to Path B; and the complex mix of wave packets appeared with different intensity and group velocities. A maximal value of S_0 mode amplitudes was obtained at 253 kHz for Path A (about 400 mV) and at 247 kHz for Path B (about 260 mV), as represented in tuning curves of Fig. 6 (b).

The differences from Path A to Path B can be due to the different orientation angle of wave propagation on the plate, and because of transducers' inconsistent bonding or misalignment, difficulty to control the thickness of the glue. Thus, signals were very complex and difficult to interpret. Consequently, DWTs were more reliable with the selectivity determined by the well-controlled electrode periodicity and the transducer consistency by printing, whereas discrete PZT transducers were biased by manual bonding installation.

In this work, fundamental modes were selected at higher frequencies when using DWTs than with PZTs. Hence smaller wavelengths can be used for active sensing, meaning smaller damage can be detected. PZTs used in this work seemed to select modes with a wavelength of 20 mm, whereas DWTs were able to select modes at customized wavelength (here, 12 mm or 10 mm). To select modes with similar wavelengths as DWTs fabricated on Plate 3, PZT length should be 6 mm or 5 mm.

D. Attenuation of A_0 mode in CFRP

A comb-shaped electrode pattern causes the wave generated to propagate mainly in the direction perpendicular to the fingers [31], [35]. This feature is very attractive for monitoring critical regions known as 'hot-spots' with highly localized stress/strain such as near fastener holes or stringers [24], [36], [37]. High directivity along the length of comb-shaped electrodes could be translated into lower wave attenuation in the direction of wave propagation because of lower wave spreading in other directions. Direction of wave propagation was compared for PZTs and DWTs using images of maximum displacement magnitudes from laser vibrometer in Supplementary Information Fig. S-2, Part III. In order to investigate the attenuation of A_0 mode, time domain displacements were obtained from the laser vibrometer every 25 mm from a transducer transmitting a five tone-burst sinusoidal signal with a Hanning window amplified to 100 Vpp. Data were collected along the path with the transducer in front: for example, data for DWT on Path A were collected along the path with the other DWT on Path A. This way, data collected for DWT were obtained with the same direction angle on the plate as for PZT, for a same path (A or B). Because the laser vibrometer gets displacement in perpendicular direction from the plate, the out-of-plane displacement was obtained, which is the main displacement of A_0 mode. The amplitude attenuation is due to geometric spreading and structural damping [28], [38]. Geometric spreading is due to the growing length of a wave front spreading into all directions from the excitation source. It can be visualized as ripples in water created by a drop and spreading into concentric circles. Structural damping is due to non-perfect elastic material behavior that implies dissipation of wave energy. By plotting displacements of the A_0 mode according to the distance from transducer, attenuation curves were obtained from fitting with the equation:

$$D(r) = \frac{D_i e^{-\alpha r}}{\sqrt{r}} \quad (2)$$

where r is the distance from the excitation source, D_i the initial displacement, and α the attenuation coefficient. This coefficient, α, is function of frequency. As reported in Table II, the attenuation coefficient of A_0 mode at 75 kHz was found at about 5 Np/m for PZTs, with displacements obtained from 10.95 µm at 25 mm. This value is close to values found in literature [28], [38]. An attenuation coefficient of A_0 mode obtained from DWTs was about 1 Np/m at 79 kHz and 98 kHz, whereas higher frequencies should be associated to higher attenuation. However, low displacements were obtained from 0.47 µm at 25 mm. Curves fitting are shown in Supplementary Information Fig. S-3, Part III. In summary, it was found that, even though the displacement amplitudes of A_0 mode generated by DWTs were very low, using the same equation for curve fitting and same angle of propagation, DWTs experienced an attenuation coefficient much lower than for PZTs.

The very low attenuation (1 Np/m) computed from DWTs displacements could be explained by the very directional wave propagation due to the electrode design. Hypothetically, the equation of geometric spreading with the square root of the distance would not influence the amplitude attenuation for DWTs as much as for PZTs. The equation for curve fitting was thus corrected by removing the part associated to geometry spreading. This can be translated into curve fitting using the equation of the structural damping only. The structural damping is given by the equation:

$$D(r) = D_i e^{-\alpha r} \quad (3)$$

where r is the distance from the excitation source, D_i the initial displacement, and α the attenuation coefficient. Attenuation coefficients in this scenario were increased to about 10 Np/m. Thereby, a more realistic value of attenuation coefficient for these frequencies (79 kHz and 98 kHz) would stand between 1 Np/m and 10 Np/m. As a result, the attenuation coefficient of A_0 mode was lower on account of the very directional propagation of waves generated by DWTs, proving the benefit of using these transducers. The results of attenuation coefficients were obtained using only 4 data points, which may interfere with results accuracy. The very low attenuation explained by a very directional wave propagation achieved by mean of electrode design can overcome low displacement

TABLE II
ATTENUATION COEFFICIENTS FOR PZTS AND DWTS ON PATH A AND PATH B OBTAINED FROM EQUATION TAKING ACCOUNT OF STRUCTURAL DAMPING AND/OR GEOMETRIC SPREADING.

		Attenuation coefficient α (Np/m)	
		Geometry spreading and structural damping, using (2)	Structural damping only, using (3)
PZT	Path A (75 kHz)	5.96	16.38
	Path B (75 kHz)	3.65	13.93
DWT	Path A (98 kHz)	1.02	10.25
	Path B (79 kHz)	0.94	9.42

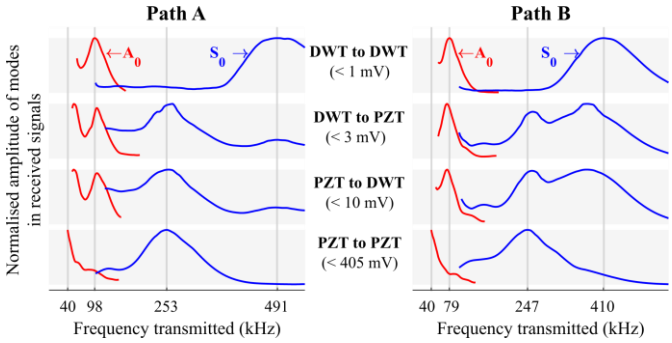

Fig. 7. Amplitudes of A_0 mode in red and S_0 mode in blue plotted according to the central frequency of the transmitted input signal for guided waves travelling between different pairs of transducers (PZT, DWT). DWTs with electrode periodicity of 10 mm on Path A and 12 mm on Path B. Frequencies selecting the modes for "DWT to DWT" and for "PZT to PZT" are represented by grey lines. In parenthesis is indicated the order of magnitudes of output signals amplitudes at their highest. The height of the eight grey background boxes indicates the [0;1] range for normalized curves.

amplitudes to improve detection sensibility and limit the influence of angle of propagation in CFRP.

IV. Direct-write transducer paired with discrete PZT transducer

It was demonstrated previously that DWTs were able to select fundamental Lamb modes, despite low amplitudes (< 1 mV). However, PZTs achieved higher amplitudes for a same 100 Vpp signal generated. By combining both transducers, their respective advantages could be united: the mode selection of DWT and the high amplitudes of PZT. The combination of DWT with PZT was studied and tuning curves of A_0 and S_0 modes are plotted in Fig. 7, for either Path A or Path B. The results for DWT to DWT and PZT to PZT are the same as plotted in Fig. 5 (b) and Fig. 6 (b) respectively. It was noted that signals for DWTs actuators with PZTs sensors (DWT to PZT) have same waveform but lower amplitudes than signals for PZT to DWT. From Fig. 7, DWTs successfully achieved the mode selection attributed to the electrode periodicity when used in combination with PZTs. Precisely, on Path A, the A_0 and S_0 modes were selected over two frequency ranges: two peaks in tuning curves. First one attributed to PZTs (low frequency for A_0 and near 253 kHz for S_0) and second one attributed to the 10 mm electrode periodicity of DWTs (98 kHz for A_0 and 491 kHz for S_0, although this second peak for S_0 was weak). Likewise, on Path B, the A_0 and S_0 modes were selected at frequencies slightly lower than for DWT to DWT: tuning curves of Path B of Fig. 7 show peaks near 79 kHz and 410 kHz slightly shifted to lower frequencies, influenced by the use of PZTs. Therefore, DWT can still achieve mode selection while paired with PZT transducers, either used as actuator or sensor.

The typical effective piezoelectric d_{33} coefficients of PZT ceramic and P(VDF-TrFE) coating are about 400 pm/V and -18 pm/V, respectively. In contrast, the typical piezoelectric g_{33} coefficients of PZT and P(VDF-TrFE) are about 25 pm/V and -380 pm/V, respectively. Therefore, PZT is powerful and more appropriate to be used as an actuator, while P(VDF-TrFE) is suitable for sensor use. Characteristic properties of DWTs are compared with that of PZTs with details presented in Supplementary Information Table S-II, Part II. The order of magnitudes of modes amplitudes at their highest point, meaning at frequencies when selecting modes, is given in parenthesis in Fig. 7. Responses were higher for PZT actuator than for DWT actuator. For a same sensor, for instance DWT, DWT to DWT modes had $1/10^{th}$ the amplitudes of modes for PZT to DWT. The DWT displayed lower amplitudes as sensor than PZT. This is because voltage responses were highly influenced by PZT resonance around 250 kHz, whereas PVDF resonance was not represented. Yet, combining PZT as actuator with DWT as sensor allowed improved signal-to-noise ratio, while selecting fundamental Lamb wave modes at specific frequencies attributed to the electrode periodicity.

V. Conclusions

Direct-write ultrasonic transducers (DWTs) were designed and fabricated by spraying piezoelectric P(VDF-TrFE) coating with comb-shaped electrodes for exciting and detecting selective guided ultrasonic waves on carbon fiber reinforced plastic (CFRP) plates. The characteristics and performance of the DWTs were investigated in comparison with discrete PZT ceramic transducers surface-mounted on the same CFRP plates. The DWTs exhibited single-mode excitation of fundamental Lamb wave A_0 or S_0 and enhanced directivity due to the comb-shaped electrode design, which was compatible with the direct-write techniques and allowed improved mode identification reliability despite the smaller signal amplitude. In contrast, influences on wave propagation of complex modes by multiple parameters such as misalignment, bonding agent, and position on the plate were observed with the manually bonded PZTs, requiring extensive signal processing and analysis. Thus, use of novel DWTs for SHM applications promises simpler signal analysis and damage interpretation. Moreover, DWTs showed improved consistency attributed to the batch fabrication by printing process. For large scale implementations, the polymeric DWTs are advantageous because they are flexible (pattern into any shapes), less intrusive (thin and lightweight), and without lead hazard. Our results also showed the combination of DWT sensor with PZT actuator could achieve balanced improvement in mode selection and signal amplitude. Further work is ongoing to study the ability and performances of DWT for impact damage detection in comparison with PZT.

References

[1] C. Soutis, "Carbon fiber reinforced plastics in aircraft construction," *Mater. Sci. Eng. A*, vol. 412, no. 1–2, 2005.

[2] V. Giurgiutiu, *Structural Health Monitoring of Aerospace Composites*. Academic Press: Waltham, MA, USA, 2016.

[3] M. O. W. Richardson and M. J. Wisheart, "Review of low-velocity impact properties of composite materials," *Compos. Part A Appl. Sci. Manuf.*, vol. 27, no. 12, 1996.

[4] G. A. O. Davies and R. Olsson, "Impact on composite structures," *Aeronaut. J.*, vol. 108, no. 1089, 2004.

[5] K. Diamanti and C. Soutis, "Structural health monitoring techniques for aircraft composite structures," *Prog. Aerosp. Sci.*, vol. 46, no. 8, 2010.

[6] L. Qiu, M. Liu, X. Qing, and S. Yuan, "A quantitative multidamage monitoring method for large-scale complex composite," *Struct. Heal. Monit.*, vol. 12, no. 3, 2013.

[7] J.-B. Ihn and F. Chang, "Pitch-catch Active Sensing Methods in Structural Health Monitoring for Aircraft Structures," *Struct. Heal. Monit.*, vol. 7, no. 1, 2008.

[8] A. Muller, C. Soutis, and M. Gresil, "Image reconstruction and characterisation of defects in a carbon fibre/epoxy composite monitored with guided waves," *Smart Mater. Struct.*, vol. 28, no. 6, 2019.

[9] Z. Su, L. Ye, and Y. Lu, "Guided Lamb waves for identification of damage in composite structures: A review," *J. Sound Vib.*, vol. 295, no. 3–5, 2006.

[10] X. Wang, Y. Lu, and J. Tang, "Damage detection using piezoelectric transducers and the Lamb wave approach: I. System analysis," *Smart Mater. Struct.*, vol. 17, no. 2, 2008.

[11] K. Diamanti, J. M. Hodgkinson, and C. Soutis, "Detection of low-velocity impact damage in composite plates using lamb waves," *Struct. Heal. Monit.*, vol. 3, no. 1, 2004.

[12] N. Salowitz, Z. Guo, Y. H. Li, K. Kim, G. Lanzara, and F. K. Chang, "Bio-inspired stretchable network-based intelligent composites," *J. Compos. Mater.*, vol. 47, no. 1, 2013.

[13] F. Kopsaftopoulos, R. Nardari, Y. H. Li, P. Wang, B. Ye, and F. K. Chang, "Experimental identification of structural dynamics and aeroelastic properties of a self-sensing smart composite wing," in *Proceedings of the 10th IWSHM*, 2015, vol. 2.

[14] J. Nunes-Pereira, P. Martins, V. F. Cardoso, C. M. Costa, and S. Lanceros-Méndez, "A green solvent strategy for the development of

piezoelectric poly(vinylidene fluoride-trifluoroethylene) films for sensors and actuators applications," *Mater. Des.*, vol. 104, 2016.
[15] N. Rajic, C. Rosalie, S. van der Velden, L. R. Francis Rose, J. Smithard, and W. K. Chiu, "A novel high density piezoelectric sensing capability for in situ modal decomposition of acoustic emissions," in *Proceedings of 9th EWSHM*, 2018.
[16] B. Ren and C. J. Lissenden, "PVDF multielement lamb wave sensor for structural health monitoring," *IEEE Trans. UFFC*, vol. 63, no. 1, 2016.
[17] B. Lin and V. Giurgiutiu, "Modeling and testing of PZT and PVDF piezoelectric wafer active sensors," *Smart Mater. Struct.*, vol. 15, no. 4, 2006.
[18] J. Bae and S. Chang, "Characterization of an electroactive polymer (PVDF-TrFE) film-type sensor for health monitoring of composite structures," *Compos. Struct.*, vol. 131, 2015.
[19] F. Bellan *et al.*, "A new design and manufacturing process for embedded Lamb waves interdigital transducers based on piezopolymer film," *Sensors Actuators, A Phys.*, vol. 123–124, 2005.
[20] S. Chen, K. Yao, F. E. H. Tay, and L. L. S. Chew, "Comparative Investigation of the Structure and Properties of Ferroelectric Poly(vinylidene fluoride) and Poly(vinylidene fluoride–trifluoroethylene) Thin Films Crystallized on Substrates," *J. Appl. Polym. Sci.*, vol. 116, no. 5, 2010.
[21] J. F. Capsal, C. David, E. Dantras, and C. Lacabanne, "Piezoelectric sensing coating for real time impact detection and location on aircraft structures," *Smart Mater. Struct.*, vol. 21, no. 5, 2012.
[22] K. Elkjaer, K. Astafiev, E. Ringgaard, and T. Zawada, "Integrated Sensor Arrays based on PiezoPaint for SHM Applications," in *Annual Conference of the Prognostics and Health Management Society*, 2013.
[23] Z. Shen, S. Chen, L. Zhang, K. Yao, and C. Y. Tan, "Direct-Write Piezoelectric Ultrasonic Transducers for Non-Destructive Testing of Metal Plates," *IEEE Sens. J.*, vol. 17, no. 11, 2017.
[24] S. Chen *et al.*, "Monitoring of cracks near fastener holes using direct-write ultrasonic transducers," *Eng. Res. Express*, vol. 2, 2020.
[25] S. Guo, S. Chen, L. Zhang, Y. F. Chen, and K. Yao, "Plastic Strain Determination With Nonlinear Ultrasonic Waves Using In Situ Integrated Piezoelectric Ultrasonic Transducers," *IEEE Trans. UFFC*, vol. 65, no. 1, 2018.
[26] S. Guo, S. Chen, L. Zhang, Y. F. Chen, M. Sharifzadeh Mirshekarloo, and K. Yao, "Design and fabrication of direct-write piezoelectric ultrasonic transducers for determining yielding of aluminum alloy," *NDT E Int.*, vol. 98, no. January, 2018.
[27] R. Lammering, U. Gabbert, M. Sinapius, T. Schuster, and P. Wierach, *Lamb-wave Based Structural Health Monitoring in Polymer Composites*, Springer. 2018.
[28] M. Gresil and V. Giurgiutiu, "Prediction of attenuated guided waves propagation in carbon fiber composites using Rayleigh damping model," *J. Intell. Mater. Syst. Struct.*, vol. 26, no. 16, 2015.
[29] M. Philibert, S. Chen, K. Yao, C. Soutis, and M. Gresil, "Direct-write piezoelectric ultrasonic transducers for impact damage detection in composite plates," in *Proceedings of 9th EWSHM*, 2018.
[30] J. L. Rose, "The upcoming revolution in ultrasonic guided waves," in *Nondestructive characterization for composite materials, aerospace engineering, civil infrastructure, and homeland security*, 2011, vol. 7983.
[31] S. T. Quek, P. S. Tua, and J. Jin, "Comparison of plain piezoceramics and inter-digital transducer for crack detection in plates," *J. Intell. Mater. Syst. Struct.*, vol. 18, no. 9, 2007.
[32] D. Schmidt, M. Sinapius, and P. Wierach, "Design of mode selective actuators for Lamb wave excitation in composite plates," *CEAS Aeronaut. J.*, vol. 4, no. 1, 2013.
[33] T. Stepinski, M. Mańka, and A. Martowicz, "Interdigital lamb wave transducers for applications in structural health monitoring," *NDT E Int.*, vol. 86, no. October 2016, 2017.
[34] Z. Su and L. Ye, *Identification of Damage Using Lamb Waves: From Fundamentals to Applications*, vol. 48. Springer Science & Business Media: Berlin, Germany, 2009.
[35] R. S. C. Monkhouse, P. D. Wilcox, and P. Cawley, "Flexible interdigital PVDF transducers for the generation of Lamb waves in structures," *Ultrasonics*, vol. 35, no. 7, 1997.
[36] A. Ataş and C. Soutis, "Subcritical damage mechanisms of bolted joints in CFRP composite laminates," *Compos. Part B Eng.*, vol. 54, no. 1, 2013.
[37] M. Philibert, C. Soutis, M. Gresil, and K. Yao, "Damage Detection in a Composite T-Joint Using Guided Lamb Waves," *Aerospace*, vol. 5, no. 2, Apr. 2018.
[38] J. Lin, F. Gao, Z. Luo, and L. Zeng, "High-Resolution Lamb Wave Inspection in Viscoelastic Composite Laminates," *IEEE Trans. Ind. Electron.*, vol. 63, no. 11, 2016.

Marilyne Philibert obtained her Master degree in technical textiles at the French engineering school ENSAIT in 2015. She is currently a final year PhD student in a joint research programme between the University of Manchester in the UK and A*STAR in Singapore. Her research interests are composite materials, SHM and piezoelectric transducers.

Shuting Chen (M'19) received his Bachelor degree in materials science and engineering and Master degree in physical chemistry of Materials from Tongji University in 2002 and 2005, respectively. He received a Ph.D degree in mechanical engineering from National University of Singapore in 2010. Currently, he is a research scientist in the Institute of Materials Research and Engineering (IMRE), A*STAR, Singapore. Prior joining IMRE in August 2013, he worked in Failure Analysis Lab of GLOBALFOUNDRIES, Singapore. His research interests are in the area of smart materials including dielectric, piezoelectric and ferroelectric materials for sensors and transducers applications.

Voon-Kean Wong (M'19) completed his B.Eng (Hons) Mechatronics Engineering from Universiti Tunku Abdul Rahman (UTAR), Malaysia, in 2012 and Ph.D. in Mechanical Engineering from The University of Nottingham Malaysia Campus, in 2018. He is currently a Research Scientist at the Institute of Materials Research and Engineering, A*STAR, Singapore. His research interests cover application of piezoelectric material for structural health monitoring and energy harvesting.

Kui Yao (M'99–SM'06) is currently a Principal Scientist, IMRE, A*STAR, Singapore, and an Adjunct Professor with Nanyang Technical University, Singapore. His research areas cover smart materials, particularly dielectric, piezoelectric, and ferroelectric materials, and the sensors and transducers enabled with these materials, including their applications for structural and condition monitoring, ultrasonic and photoacoustic nondestructive testing and diagnosis, noise and vibration mitigation.

The manuscript is published: Marilyne Philibert, Shuting Chen, Voon-Kean Wong, Kui Yao, Constantinos Soutis, and Matthieu Gresil, “Direct-write piezoelectric transducers on carbon-fiber reinforced polymer structures for exciting and receiving guided ultrasonic waves,” IEEE Transactions on Ultrasonics, Ferroelectrics, and Frequency Control, DOI: 10.1109/TUFFC.2021.3073131, Vol. 68, No. 8, pp. 2733-2740, 2021.

Constantinos Soutis PhD(Cantab) is Professor of Aerospace Engineering and Head of the Aerospace Research Institute at the University of Manchester (UK). His research focuses on damage mechanics of composite materials and structural health monitoring. He has authored or co-authored more than 400 ISI listed papers and successfully supervised over 40 PhD students. He is a Chartered Engineer and a Fellow of the UK Royal Academy of Engineering, distinguished for his major contributions to the science and technology of the mechanics and mechanisms of failure of fibre-composite materials based upon polymeric matrices. The Academy's Fellows represents the nation’s best engineering researchers, innovators, entrepreneurs, business and industry leaders. Election to the Academy is by invitation only.

Matthieu Gresil (Dr) is a Senior Lecturer in the Department of Materials Science and Engineering and the Department of Mechanical and Aerospace Engineering at Monash University. He established and lead the advanced multi-functional composite materials group in the i-Composites Lab. His interdisciplinary research group is focused on (i) multifunctionality that could be built into a composite structure, such as self-healing, reprocessing, recycling, health monitoring, and thermal-load dissipation; (ii) emerging polymer materials such as vitrimers which can heal and morph with a thermal trigger; and (iii) bio-inspired 2D/3D morphing materials using printing technology and nanotechnology.